Multiphonon resonant Raman scattering in nanocrystals

R. Rodríguez-Suárez* and E. Menéndez-Proupin[†]

Departamento de Física Teórica, Universidad de La Habana, Vedado 10400, La Habana, Cuba

C. Trallero-Giner[‡] and M. Cardona

Max-Planck-Institut für Festkörperforschung, Heisenbergstrasse 1, D-70569 Stuttgart, Federal Republic of Germany

(Received 15 March 2000)

We have studied the multiphonon resonant Raman scattering from confined and interface polar optical phonons in spherical nanocrystallites. The intermediate virtual states in the scattering process are taken into account as Wannier-Mott confined excitons in a spherical dot. Fröhlich interaction between excitons and optical phonons has been considered and general selection rules for the exciton-phonon matrix elements and multiphonon scattering processes in the case of spherical quantum dots have been derived. It is shown that for a second-order process, two phonons are created with the same angular momentum ($l_{p_1} = l_{p_2}$) while, in a third-order process, the second emitted (or absorbed) phonon with angular momentum l_{p_2} must fulfill the triangular property $|l_{p_1} - l_{p_3}| \leq l_{p_2} \leq l_{p_1} + l_{p_3}$. In the general case, the sum of phonon momentum projections on the z axis $m_{p_1} + m_{p_2} + \cdots = 0$. We have performed multiphonon Raman cross-section calculations of CdSe quantum dots of various sizes up to third order and present detailed comparison with available experimental data. The effect of size distribution is studied; we show that a broad dispersion of nanocrystal sizes has important consequences on the multiphonon Raman spectra. The experimental relative intensities between phonon overtones are correctly described in the framework of the present model. Also, an analysis of the applicability of the Huang-Rhys factor for quantum dot systems is presented and several contradictions found in the literature concerning this parameter have been explored.

I. INTRODUCTION

During the last two decades semiconductor nanocrystals have been thoroughly investigated with regards to their promising applications in technology of optical devices[1] and, recently, as biological probes in combination with organic molecules.[2] Their applicability and diversity comes from their singular optical properties, which depend strongly on size and geometrical factors. On the other hand, the possibility of making very small crystallites at relatively low cost makes them useful systems for the investigation of quantum confinement effects on the elementary excitations of semiconductors. Their main drawback as a research object is their broad size distribution in a real sample, which obscures the properties of individual nanocrystals. Nevertheless, important progress has been made in several directions: (1) Development of techniques that yield nanocrystals with well-defined and controllable size distributions;[3–6] (2) Implementation of microluminescence and micro-Raman measurements that allow the observation of individual or only a few quantum dots,[7,8] (3) Use of size selective spectroscopic techniques as holeburning[9] and Raman scattering.[10] Several works in the late 80's and early 90's focused on the electron-phonon coupling strength in CdSe quantum dots,[11–15] giving some contradictory results. In particular, in Ref. 14 it is shown that the coupling strength between phonons[16] and intrinsic confined excitons is much smaller than that obtained from multiphonon Raman experiments interpreted in terms of the Franck-Condon theory. The same result is obtained in PbS nanocrystals.[17] To avoid this problem, and to achieve better agreement between theory and experiments, other interactions have been incorporated in the theory.[14,15,18] Multiphonon resonant Raman scattering (MRRS) provides a useful tool to investigate the Fröhlich-type exciton-lattice interaction in quantum dot (QD) nanostructures. First-order Raman and hyper-Raman scattering only provide information about spherical (phonon angular momentum $l_p = 0$) and nonspherical symmetry ($l_p = 1$) modes, respectively, while the MRRS gives rise to the confined and interface optical modes with $l_p > 1$. These are confirmed by Raman spectroscopy of CdSe, (Refs. 12 and 13) PbS (Ref. 17) and CdS (Ref. 19) nanocrystals. In the past, high-order Raman spectra have been extensively studied in bulk Group-II–VI semiconductors (see Ref. 20) as well as in quantum well systems (see Ref. 21). It has become clear that a combined scattering mechanism for MRRS involving all excitonic states leads to a strong increase of the scattering efficiency, in particular to strong outgoing resonances. A MRRS process is strongly dependent on the exciton-phonon coupling, and should be a useful tool to investigate the optical lattice vibrations and their interaction with the electronic states of nanocrystals. The strength of the exciton-phonon interaction is manifested by a set of overtones at integer multiples of the LO phonon frequency. The observed multiphonon spectra of semiconductor microcrystallites are rather similar to those obtained in bulk semiconductors, although the relative intensities of MRRS overtones are very sensitive to the radii of the QD's.[13,19]

In this paper we present a theoretical model that allows us to study multiphonon Raman scattering by optical polar vibrational modes and compare the theoretical predictions with available Raman spectra of CdSe QD's. Since the Fröhlich interaction becomes the strongest coupling mechanism in polar semiconductor microcrystallites for incoming light photon energy in resonance with excitonic states, only this exciton-phonon coupling will be considered here. Through a detailed calculation of the matrix elements and the selection rules involved in the scattering process, we provide a quan-

titative analysis of MRRS in spherical nanocrystals. We present microscopic calculations of the resonant Raman cross sections, which take into account the relevant diagrams of the high-order scattering processes and investigate the relative overtone intensities, their dependence on dot radius, and the resonance profile for CdSe quantum dots embedded in a glass matrix.

II. THEORY

A. General formalism

The MRRS process consists of the following steps: the exciting photon of frequency ω_l creates an electron-hole pair (exciton), this exciton is scattered through generation of k optical phonons and, finally, it recombines with the emission of a photon of frequency $\omega_s = \omega_l - k\omega_{LO}$. For the zero-dimensional case and a kth-order process the observed $k\omega_{LO}$ line is due to a combination of k vibrational excitations of frequency ω_{p_j} ($j = 1, 2, \ldots k$). Typical diagrams contributing to the second- and third-order scattering amplitudes in a QD are shown in Fig. 1.

The MRRS cross section[22] of a quantum dot can be written as:

$$\frac{d^2\sigma}{d\Omega d\omega_s} = \frac{V^2 \omega_s^3 \eta_l \eta_s^3}{4\pi^2 c^4 \omega_l N_l \hbar}$$

$$\times \sum_F |W_{FI}(\omega_s, \mathbf{e}_s; \omega_l, \mathbf{e}_l)|^2 \delta(E_F - E_I), \quad (1)$$

where c is the velocity of light in vacuum, V a normalization volume $\eta_l(\eta_s)$, and $\mathbf{e}_l(\mathbf{e}_s)$ are the refractive index and the unit polarization vector of the incident (scattered) light, respectively. W_{FI} is the scattering amplitude for the transition from the initial state $|I(\omega_l, \mathbf{e}_l)\rangle$ to the final state $|F(\omega_s, \mathbf{e}_s)\rangle$. Under the conditions found in Raman experiments with semiconductor quantum dots, assuming $T = 0$ K, and in the framework of the adiabatic approximation, the initial state $|I\rangle$ is given by $|N_l, 0_s\rangle \otimes |0_{p_1}, 0_{p_2}, \ldots\rangle \otimes |G\rangle$, while the final state $|F\rangle$ is equal to $|N_l - 1, 1_s\rangle \otimes |n_{p_1}, n_{p_2}, \ldots\rangle \otimes |G\rangle$. Here, $|0\rangle$ and $|G\rangle$ represent the ground state of the vibrational and electronic fields, respectively. On the other hand, N_j ($j = l, s$) and n_p are the occupation numbers of photons $|j\rangle$
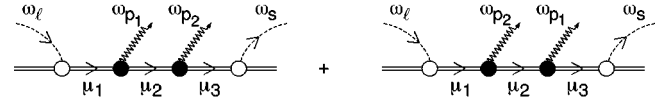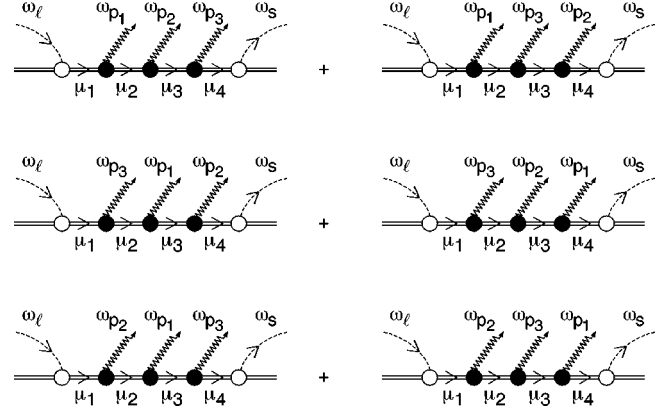

FIG. 1. Topologically nonequivalent resonance diagrams contributing to the scattering amplitude in the case of: (a) Second-order Raman scattering processes and (b) Third-order processes. The virtual intermediate excitonic states are labeled by μ and the vibrational excitation frequencies by ω_p. Empty circles represent the exciton-radiation interaction, the filled circles the exciton-lattice interaction in the QD. The sum of these diagrams for the particular case when in the final state identical LO vibrons participate can be carried out following Eq. (5).

$= |\mathbf{e}_j, \mathbf{k}_j\rangle$ with polarization vector $\mathbf{e}_j$ and wave vector $\mathbf{k}_j$, and of optical vibrational modes $|p\rangle$ with frequency ω_p, respectively. Energy conservation imposes the restriction

$$E_I - E_F = \hbar\omega_l - \hbar\omega_s - \sum_{j=1}^{k} \hbar\omega_{p_j}. \quad (2)$$

The corresponding scattering amplitude can be obtained from time-dependent perturbation theory, considering the interaction Hamiltonian as a sum of the exciton-radiation ($\hat{H}_{E-R}$) and exciton-lattice ($\hat{H}_{E-L}$) operators. Under resonance conditions, the leading term in the scattering amplitude is[23]

$$W_{FI}^{(k)} = \sum_{V_1, \ldots V_{k+1}} \frac{\langle F|\hat{H}_{E-R}|V_{k+1}\rangle \left[\prod_{j=1}^{k} \langle V_{j+1}|\hat{H}_{E-L}|V_j\rangle \right] \langle V_1|\hat{H}_{E-R}|I\rangle}{\left[\prod_{j=0}^{k} (E_I - E_{V_{j+1}}) \right]}.$$

The virtual intermediate states of the radiation+vibration +electron fields are described by the ket $|V_j\rangle = |N_l - 1, 0_s\rangle \otimes |n_{p_1}, \ldots, n_{p_j} - 1, 0, \ldots\rangle \otimes |\mu_j\rangle$ and an energy $E_{V_j} = (N_l - 1)\hbar\omega_l + \Sigma_{n=1}^{j} \hbar\omega_{p_n} + E_{\mu_j}$, where the excitonic states are given by $|\mu\rangle$ and energy E_μ. The sum over V_j states takes

into account all possible diagrams obtained by permuting the phonon interaction vertices. For a given kth order process the sum is confined to the appropriate number of nonequivalent Feynman diagrams (see Fig. 1 for a second- and third-order processes). The above expression can be reduced to the usual

notation with solely matrix elements between the states μ_j of the electronic subsystem if the matrix elements $\langle V_{j+1}|\hat{H}_{E-L}|V_j\rangle$ are rewritten as

$$\langle V_{j+1}|\hat{H}_{E-L}|V_j\rangle = \langle \mu_{j+1}|H_{E-L}^{(p_j)}|\mu_j\rangle\langle n_{p_j}|b_{p_j}^{\dagger}|n_{p_j}-1\rangle$$

$$= \sqrt{n_{p_j}}\langle \mu_{j+1}|H_{E-L}^{(p_j)}|\mu_j\rangle. \qquad (3)$$

$H_{E-L}^{(p_j)}$ is associated to the phonon creation operator $b_{p_j}^{\dagger}$ with quantum numbers p_j and the excitonic transition $|\mu_j\rangle \rightarrow |\mu_{j+1}\rangle$. For the final vibrational state $|n_{p_1}, n_{p_2}, \ldots n_{p_r}\rangle$ with the condition $n_{p_1}+n_{p_2}+ \ldots +n_{p_r}=k$, we have

$$W_{FI}^{(k)}=(n_{p_1}!n_{p_2}!\ldots n_{p_r}!)^{1/2}(N_l)^{1/2}\sum_{P_e}\hat{P}_e M_{FI}(p_1, \ldots,p_k),$$

$$M_{FI}(p_1, \ldots,p_k)= \sum_{\mu_1, \ldots \mu_{k+1}} \frac{\langle G|H_{E-R}^{+}|\mu_{k+1}\rangle\left[\prod_{j=1}^{k}\langle \mu_{j+1}|H_{E-L}^{(p_j)}|\mu_j\rangle\right]\langle \mu_1|H_{E-R}^{-}|G\rangle}{\left[\prod_{j=1}^{k}\left(\hbar\omega_l - E_{\mu_{j+1}} - \sum_{n=1}^{j}\hbar\omega_{p_n} + i\Gamma_{\mu_{j+1}}^{ex}\right)\right](\hbar\omega_l - E_{\mu_1} + i\Gamma_{\mu_1}^{ex})}. \qquad (4)$$

Here, H_{E-R}^{+} (H_{E-R}^{-}) denotes the exciton-radiation Hamiltonian interaction operator associated to the photon creation (annihilation). $\hat{P}_e$ is the operator of permutations of the indices $p_1, \ldots,p_k$ and the sum with index P_e runs over all nonequivalent permutations. In the sense of Feynman diagrams it corresponds to the sum over topologically nonequivalent diagrams. The factor $(n_{p_1}!n_{p_2}!\ldots n_{p_r}!)^{1/2}$ arises when in the final state at least one vibrational excitation is excited several times. The product of all factors $\sqrt{n_{p_j}}$ is equal to $(n_{p_1}!n_{p_2}!\ldots n_{p_r}!)^{1/2}$.

The sum over the final states is essentially a sum over multiphonon states. In an operational sense, one needs to sum over the nonequivalent sets $\{p_1,p_2, \ldots,p_k\}$, where the order of the vibrational excitation labels p's is irrelevant. To express the sum in terms of the p's without repeating terms, we replace the sum in Eq. (4) by

$$\sum_{F=\{p_1,p_2, \ldots,p_k\}}|W_{FI}^{(k)}|^2\delta(E_F-E_I)$$

$$= N_l\sum_{p_1\leqslant p_2\leqslant \ldots \leqslant p_k}(n_{p_1}!n_{p_2}!\ldots n_{p_r}!)^{-1}$$

$$\times \left|\sum_{P_e'}\hat{P}_e' M_{FI}(p_1, \ldots,p_k)\right|^2\delta(E_F-E_I),$$

where now P_e' are all the permutations between the labels p's, including exchange of equal labels. The change from the sum over nonequivalent permutations P_e to the sum over all permutations P_e' is effected by means of a factor $(n_{p_1}!n_{p_2}!\ldots n_{p_r}!)^{-1}$, obtained from elemental combinatorial analysis. We can replace the ordered p's sum by the whole sum using

$$\sum_{F=\{p_1,p_2, \ldots,p_k\}}|W_{FI}^{(k)}|^2\delta(E_F-E_I)$$

$$= \frac{N_l}{k!}\sum_{p_1,p_2, \ldots,p_k}\left|\sum_{P_e'}\hat{P}_e' M_{FI}(p_1, \ldots,p_k)\right|^2\delta(E_F-E_I). \qquad (5)$$

Equation (5), although computationally expensive, is structurally simpler as we do not need to watch out for identical phonons.

By examining Eq. (4) it is found that the relevant resonances for a kth-order process will occur at $\hbar\omega_l = E_{\mu_1}$ (incoming resonance), $\hbar\omega_l = E_{\mu_{k+1}} + \Sigma_{n=1}^{k}\hbar\omega_{p_n}$ (outgoing resonance), and a series of intermediate resonances at $\hbar\omega_l = E_{\mu_{j+1}} + \Sigma_{n=1}^{j}\hbar\omega_{p_n}$, where each p_n can occur several times.

B. Selection rules for spherical nanocrystals

In the following we consider quantum dots with spherical shape and radius R. The electronic subsystems are taken to be Wannier-Mott excitons confined in the QD and treated in the framework of the effective-mass approximation. The excitonic states $|\mu\rangle$ are labeled by the quantum numbers N,L,M, and P, corresponding to the energy, the square of the orbital angular momentum, its projection over a quantization axis, and the parity, respectively. Notice that N, L, M, and P are related only to the envelope of the exciton wave function, not to its Bloch part. The eigenstates $|N,L,M,P\rangle$ of the effective-mass equation are expanded in terms of electron-hole states $|\alpha,L,M,\rangle$

$$|N,L,M,P\rangle = \sum_{\alpha}C_{N,L,M,P}(\alpha)|\alpha,L,M\rangle, \qquad (6)$$

where α denotes the set of quantum numbers of the uncorrelated electron-hole states. The eigenstates $|\mu\rangle$ and the excitonic energies E_μ are obtained by numerical diagonalization of the Wannier-Mott Hamiltonian. The details of this approach are given elsewhere.[24,25]

In polar semiconductors the Fröhlich mechanism is allowed for MRRS, playing the dominant role in the scattering efficiency. In the following we shall only deal with the Fröhlich interaction induced Raman scattering. The vibrational optical modes will be treated within the formalism of Refs. 25 and 26, where a phenomenological continuous model is developed to describe the vibrational states of a QD. The polar optical vibrations are described with the help of a vec-

tor field **u** coupled to a scalar field ϕ, which represent the cation-anion relative displacement and the concomitant long-range electrostatic potential, respectively. The normal modes, of frequency ω_p, are labeled by the set $p = (n_p, l_p, m_p)$, with l_p and m_p representing angular momentum and its projection, respectively. The exciton-LO phonon interaction Hamiltonian $\hat{H}_{E-L} = e[\varphi_F(\mathbf{r}_e) - \varphi_F(\mathbf{r}_h)]$, where $\mathbf{r}_e (\mathbf{r}_h)$ are the electron(hole) coordinates and φ_F is equal to

$$e\varphi_F(\mathbf{r}) = \frac{C_F}{\sqrt{R}} \sum_{n,l,m} \sqrt{\frac{\omega_L}{\omega_{n.l}}} \Phi_{n,l}(r) Y_{l,m}(\Omega) b_{n,l,m} + \text{H.c.,}$$

(7)

C_F is the Fröhlich constant, $Y_{l,m}$ ($-l \leq m \leq l$) the spherical harmonics, and $\Phi_{n,l}(r)$ the radial part of the potential. Details of these calculations are given elsewhere.[26,27]

Due to the spherical symmetry, several selection rules arise associated with angular momentum conservation. The matrix element $\langle \mu | H_{E-R}^- | G \rangle = \langle G | H_{E-R}^+ | \mu \rangle^*$ for direct-allowed transitions between c and v bands is given by

$$\langle \mu | H_{E-R}^+ | G \rangle = \frac{e}{m_0} \sqrt{\frac{2\pi\hbar}{\omega\eta^2}} \frac{\mathbf{e} \cdot \mathbf{p}_{cv}}{\sqrt{V}} \delta_{L,0} \delta_{M,0} \delta_{P,1}$$

$$\times \sum_{n,l} (-1)^l \sqrt{2l+1} C_{N,0,0,1}(n,n,l,l).$$

(8)

In the above equation the radial part of the single-particle states was assumed to be that of the spherical dot with an infinite barrier.[24] The excitons μ_1 and μ_{k+1}, which mediate the interaction with the radiation field in Eq. (4), have zero angular momentum ($L_1 = L_{k+1} = 0$) and even parity ($P_1 = P_{k+1} = 1$).

The calculation of the interaction matrix elements $\langle \mu_i | H_{E-L}^{(p)} | \mu_j \rangle$ for excitons and phonons with arbitrary L and l_p angular momenta, involve a sum of Clebsch-Gordan coefficients over the electron and hole magnetic quantum numbers $(m_{e_i}, m_{h_i}, m_{e_j}, m_{h_j})$. This sum can be performed with the help of the diagrammatic technique of Brink and Satcher[28] or alternatively, with the help of the Wigner-Eckart theorem. For a discussion of these calculations see the Appendix of Ref. 25. The obtained matrix elements have the following explicit expression:

$$\langle \mu_i | H_{E-L}^{(p)} | \mu_j \rangle = \frac{C_F}{\sqrt{4\pi R}} \sqrt{(2L_i+1)(2L_j+1)(2l_p+1)} (-1)^{-M_j} \begin{pmatrix} L_i & l_p & L_j \\ -M_i & -m_p & M_j \end{pmatrix} \sum_{\alpha_i, \alpha_j} C_{\mu_i}^*(\alpha_i) C_{\mu_j}(\alpha_j)$$

$$\times \left[(-1)^{l_{e_j}} \delta_{n_{e_i}, n_{e_j}} \delta_{l_{e_i}, l_{e_j}} \sqrt{(2l_{h_i}+1)(2l_{h_j}+1)} \begin{pmatrix} l_{h_i} & l_p & l_{h_j} \\ 0 & 0 & 0 \end{pmatrix} \begin{Bmatrix} L_i & L_j & l_p \\ l_{h_j} & l_{h_i} & l_{e_j} \end{Bmatrix} \langle n_{h_i}, l_{h_i} | \Phi_{n_p, l_p} | n_{h_j}, l_{h_j} \rangle \right.$$

$$- (-1)^{l_{h_j} + L_i + L_j + l_p} \delta_{n_{h_i}, n_{h_j}} \delta_{l_{h_i}, l_{h_j}} \sqrt{(2l_{e_i}+1)(2l_{e_j}+1)}$$

$$\left. \times \begin{pmatrix} l_{e_i} & l_p & l_{e_j} \\ 0 & 0 & 0 \end{pmatrix} \begin{Bmatrix} L_i & L_j & l_p \\ l_{e_j} & l_{e_i} & l_{h_j} \end{Bmatrix} \langle n_{e_i}, l_{e_i} | \Phi_{n_p, l_p} | n_{e_j}, l_{e_j} \rangle \right].$$

(9)

Equation (9) contains implicitly the selection rules for the matrix elements of the exciton-phonon interaction $\langle \mu_{j+1} | H_{E-L}^{(p_j)} | \mu_j \rangle$. From the properties of the 3-j symbol of the top line of Eq. (9) we derive

$$|L_j - L_{j+1}| \leq l_{p_j} \leq L_j + L_{j+1},$$

(10)

$$M_{j+1} = M_j - m_{p_j},$$

(11)

for $j = 1, \ldots, k$. The parity selection rule follows from the properties of the 3-j symbols inside the parentheses. For example, the first term

$$\begin{pmatrix} l_{h_i} & l_p & l_{h_j} \\ 0 & 0 & 0 \end{pmatrix}$$

tells that $l_{h_i} + l_p + l_{h_j}$ must be even while the Kronecker delta determines that $l_{e_i} = l_{e_j}$, therefore $(-1)^{l_{e_i} + l_{h_i}} \times (-1)^{l_{e_j} + l_{h_j}} = (-1)^{l_p}$. Hence, the parity selection rule for the exciton-phonon interaction is:

$$P_j P_{j+1} = (-1)^{l_{p_j}} \quad j = 1, \ldots, k.$$

A general selection rule for the emitted phonons in the QD reads

$$\sum_{j=1}^{k} m_{p_j} = 0.$$

(12)

Combining the above equations and the dipolar selection rules $L_1 = L_{k+1} = 0$, $P_1 = P_{k+1} = 1$, allows us to find the constraints for the phonons and excitons taking part in the MRRS processes (see Table 1).

Figure 2 displays the dimensionless matrix elements $\langle L = l_p, N = 1 | h_{E-L}^{(p_j)} | N = 1, L = 0 \rangle = \langle L = l_p, N = 1 \times | H_{E-L}^{(p_j)} \sqrt{4\pi R}/C_F | N = 1, L = 0 \rangle$ of the exciton-phonon interaction Hamiltonian as a function of the QD radius for several l_p, n_p vibrational modes. For the numerical calculations the parameters of CdSe dots in a glass matrix of Ref. 25 were used. In Fig. 2 we see that the principal contribution to the $N = 1$ matrix element comes from the phonon states with

TABLE I. Phonon selection rules for a MRRS process in a spherical quantum dot. The allowed virtual exciton transitions are also indicated.

Order	Phonon	Exciton
First	$l_{p1} = m_{p1} = 0$	$\|N_1, L_1 = 0, M_1 = 0, P_1 = 1\rangle \rightarrow$
		$\|N_2, L_2 = 0, M_2 = 0, P_2 = 1\rangle$
Second	$l_{p_1} = l_{p_2} = l_p$	$\|N_1, L_1 = 0, M_1 = 0, P_1 = 1\rangle \rightarrow$
	$m_{p_1} = -m_{p_2} = -m_p$	$\|N_2, L_2 = l_p, M_2 = m_p, P_2 = (-1)^{l_p}\rangle \rightarrow$
		$\|N_3, L_3 = 0, M_3 = 0, P_3 = 1\rangle$
Third	$\|l_{p_1} - l_{p_3}\| \leqslant l_{p_2} \leqslant l_{p_1} + l_{p_3}$	$\|N_1, L_1 = 0, M_1 = 0, P_1 = 1\rangle \rightarrow$
	$l_{p_1} + l_{p_2} + l_{p_3} = \text{even}$	$\|N_2, L_2 = l_{p_1}, M_2 = -m_{p_1}, P_2 = (-1)^{l_{p_1}}\rangle \rightarrow$
	$m_{p_1} + m_{p_2} + m_{p_3} = 0$	$\|N_3, L_3 = l_{p_3}, M_3 = m_{p_3}, P_3 = (-1)^{l_{p_3}}\rangle \rightarrow$
		$\|N_4, L_4 = 0, M_4 = 0, P_4 = 1\rangle$

$l_p = 1, 2, 3$, and $n_p = 1$ and, throughout the radius range under consideration, the largest contribution corresponds to the $n_p = 1, l_p = 1$ mode. The maximum observed for $n_p = 3$ at certain radii is identified as related to the so-called Fröhlich mode ($l_p = 1$) and to *surface modes* ($l_p = 2$ and 3).[26] At radii where the mode frequencies ω_{l_p, n_p} are closer to the Fröhlich frequency ω_F ($1.5 \leqslant R \leqslant 2.0$ nm) or to the surface frequency ω_l (the maxima are at $R \sim 1.7$ nm for $n_p = 2, l_p = 2$, $R \sim 2.1$ nm for $n_p = 3, l_p = 2$, and $R \sim 2.5$ nm for $n_p = 3, l_p = 3$) the electrostatic potential will increase, increasing the absolute value of the exciton-phonon matrix elements. It is precisely in this range that these modes present a mixed interface-confined character. Other conclusions follow from Fig. 2: (a) the matrix element $\langle \mu_{j+1} | H_{E-L}^{(p_j)} | \mu_j \rangle$ drops off rapidly for $n_p > 1$, (b) the contributions of the $l_p = 0$ modes to the MRRS ($k \geqslant 2$) cross section are very small, and (c) the dominant role is played by the $l_p = 1$ phonons.

III. RAMAN CROSS SECTION

Nanocrystals embedded in a glass or an organic matrix present a distribution in size and shape. For a specific incoming photon energy we need to calculate the average Raman cross section of the dots that fulfill any of the resonance conditions. The corresponding expression for the average Raman cross section is[10,25]

$$S_D = \int \frac{d^2\sigma(R)}{d\Omega d\omega_s} F(R) dR = \sum_r \frac{d^2\sigma(R_r)}{d\Omega d\omega_s} F(R_r) \frac{\pi \Gamma_r}{dE_r/dR_r},$$

(13)

where a Gaussian size distribution function $F(R)$ with mean radius R_m and full width at half maximum (FWHM) σ, is assumed. $\{E_r\}$ is the set of resonant exciton levels for a radius $R = R_r$.

A. Second-order process

The selection rules obtained in Sec. II, Eq. (5) for a second-order process can be reduced to

$$\sum_F |W_{FI}^{(2)}|^2 \delta(E_F - E_I)$$

$$= \frac{1}{2N_l} \sum_{n_{p_1}, n_{p_2}, l_p} (2l_p + 1) |M_{FI}(p_1, p_2)$$

$$+ M_{FI}(p_2, p_1)|^2 \frac{\Gamma_2/\pi}{(\omega_l - \omega_s - \omega_{l_p, n_{p_1}} - \omega_{l_p, n_{p_2}})^2 + \Gamma_2^2},$$

(14)

where a Lorentzian function replaces the delta function appearing in Eq. (5) and $\Gamma_2 = \Gamma_{p_1} + \Gamma_{p_2}$ is the total phonon linewidth taking place in the process.

Figure 3(a) displays the average second-order Raman cross section of an ensemble of CdSe nanocrystals for a laser photon energy $\hbar\omega_l = 2.5716$ eV. The squares represent experimental data taken from a commercial filter of CdSe nanocrystallites with a Gaussian size distribution function with average radius $R_m = 1.9$ nm [for $R_m = 4.0$ nm see Fig. 3(b)] and a $\sigma = 0.1 R_m$ FWHM. For the exciton linewidth we chose $\Gamma_0^{ex} = 5$ meV (see Ref. 1) and $\Gamma_1^{ex} = 15$ meV [$\Gamma_1^{ex} = 8$ meV in Fig. 3(b)] for the ground and excited states, respectively.[29] R_m was estimated from the maximum of the absorption coefficient with the formula $E(R_m) = \hbar^2 \pi^2 / 2\bar{\mu} R_m^2$ (where $\bar{\mu}$ is the reduced exciton mass) for the electron-hole pair confinement energy.[13] The line represents our theoretical calculation for which $\Gamma_{p_1} = \Gamma_{p_2} = 11$ cm^{-1} ($\Gamma_{p_1} = \Gamma_{p_2} = 6$ cm^{-1} for $R_m = 4.0$ nm) has been assumed following the reported experimental data.[13] The bulk energy gap relevant to the nanocrystal has been estimated from the E_g gap of CdSe at 4 K (Ref. 10) and the temperature derivative $dE_g/dT = -3.6 \times 10^{-4}$ eV/K.[30] The Raman cross section is dominated by $l_p = 1$ vibrational excitations. The main peak in Fig. 3(a) is due to the creation of two confined phonons with quantum numbers $p_1 = (l_p = 1, n_p = 1, m_p)$ and $p_2 = (l_p = 1, n_p = 1, -m_p)$, where $m_p = 0, \pm 1$ and smaller contributions from states with $l_p = 0, 2$, and 3. The other feature of the measured spectrum is a shoulder at ~ 400 cm^{-1}, which is likely to be due to scattering me-
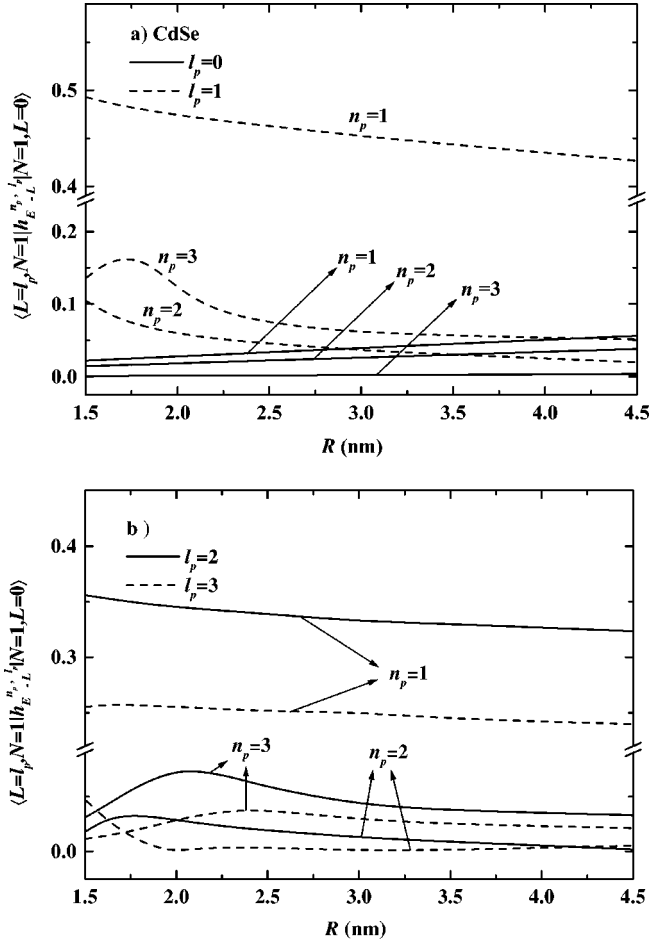
FIG. 2. Dimensionless matrix elements $\langle L=l_p, N=1 | h_{E-L}^{l_p, n_p} | N=1, L=0 \rangle$ contributing to the MRRS processes as a function of the QD radius for several l_p, n_p vibrational states. (a) $l_p=0$ (solid lines) and $l_p=1$ (dashed lines). (b) $l_p=2$ (solid lines) and $l_p=3$ (dashed lines). The maxima for $n_p=3$, $l_p=1$, 2, and 3 correspond to the radii where the ω_{l_p, n_p} are near "surface phonon" frequencies ω_l ($l=1,2$, and 3).
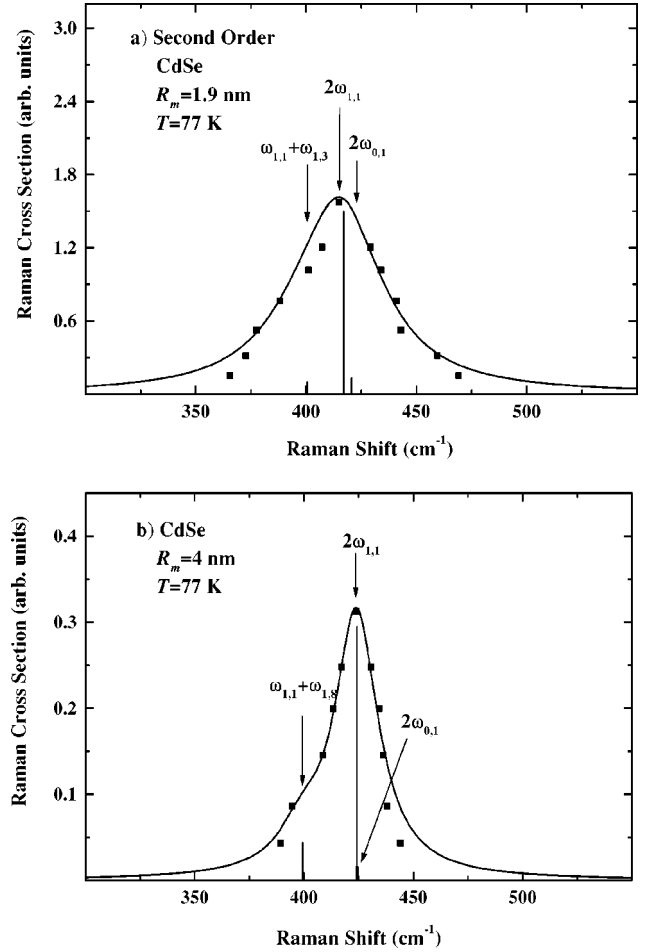
FIG. 3. Second-order Raman cross section of an ensemble of CdSe nanocrystals embedded in glass. Theory: solid line, experiment: black squares. The ensemble of dots has a Gaussian size distribution function with 10% FWHM. (a) Spectra at $\hbar\omega_l=2.572$ eV and mean radius $R_m=1.9$ nm. (b) $\hbar\omega_l=2.184$ eV and $R_m=4.0$ nm. The main contributions and their relative strengths are labelled by arrows and vertical lines, respectively.

diated by a confined phonon $\omega_{1,1}$ and a mixed confined-interface phonon $\omega_{1,3}$. However, the shoulder predicted by the theory is weaker and is located at a higher frequency than the experimental one. The latter corresponds to the Fröhlich phonon of the dielectric model, which does not strictly apply when mechanical confinement effects are present.[26,31] In order to clarify the discussion about the different scattering contributions we need to look back to Fig. 2 where the electron-phonon matrix elements relevant to the creation of individual phonons (n_p, l_p) are displayed. In the second-order scattering, the product of the two H_{E-L} matrix elements does not depend on m_p, and we only need to analyze the strength of the n_p, l_p scattering channels. In Fig. 2 it is shown that the $l_p=1$, $n_p=1$ phonons possess the largest matrix elements throughout the radius range under consideration. Other states with a significant contribution are $l_p=2$ and 3 with $n_p=1$. On the other hand, the $l_p=1$, $n_p=3$ matrix element has large values in the $R\sim1.5-2.0$ nm range, explaining the observed shoulder in Fig. 3(a). It is precisely in this range of radii where the mode $l_p=1$, $n_p=3$ presents a mixed interface-confined character and its frequency $\omega_{1,3}$ is close to the Fröhlich frequency ω_F. The spectrum of Fig.

3(a) is the result of contributions of nanocrystals in different resonance regimes: Incoming resonance for $R_1=1.96$ nm, intermediate resonance for $R_2=2.0$ nm, and outgoing resonance for $R_3=2.04$ nm, all of them with the $|N=1, L=1, M, P=-1\rangle$ excitonic level. Resonances with higher exciton states occur for larger R values but are quenched by the size distribution function used in our calculation.

Figure 3(b) shows the average second-order Raman cross section of an ensemble of nanocrystals with $R_m=4.0$ nm and $\sigma=0.1R_m$ for a laser energy $\hbar\omega_l=2.184$ eV, along with the experimental data of Ref. 13. Our calculation reproduces quite well the asymmetric line shape and attributes the shoulder at 399 cm^{-1} to scattering by the combination of the two phonons $\omega_{1,1}$ and $\omega_{1,8}$. The $\omega_{1,8}$ corresponds to the mixed confined-interface mode for $R\sim4$ nm. The nanocrystals that contribute to the average cross section of Fig. 3(b) have resonance radii equal to $R_1=3.93$ nm (incoming resonance), $R_2=4.08$ nm (intermediate resonances), and $R_3=4.26$ nm (outgoing resonance). The weights of the main contributions to the Raman cross section are illustrated in Figs. 3(a) and 3(b) by vertical lines. These lines indicate the relative strength of the confined-interface modes.
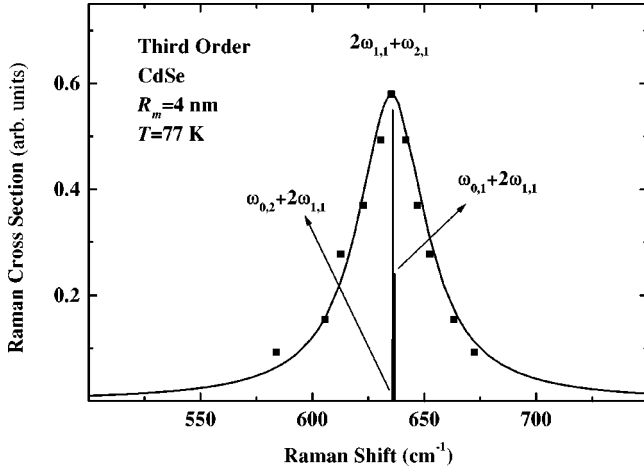
FIG. 4. The same as Fig. 3 for the third-order Raman cross section at $\hbar\omega_l = 2.184$ eV of an ensemble of nanocrystals with $R_m = 4.0$ nm and 10% FWHM dispersion radius.

B. Third-order processes

Using Eq. (5) and the obtained selection rules we are able to evaluate the third-order Raman spectrum by taking into account all allowed $\omega_{p_1} + \omega_{p_2} + \omega_{p_3}$ combinations contributing to the cross section. Figure 4 shows the average third-order Raman cross section of CdSe nanocrystals for the same laser frequency as Fig. 3(b) ($\hbar\omega_l = 2.184$ eV). This spectrum has been calculated for a Gaussian radius distribution function with a 4.0-nm mean radius and $\sigma = 0.1R_m$. In the calculation, phonon linewidths of $\Gamma_{p_1} = \Gamma_{p_2} = \Gamma_{p_3} = 6$ cm^{-1} have been used to fit the experimental data. We found that the main peak is due to the contribution of three phonons with frequencies $\omega_{l_1=1,n_1=1} + \omega_{l_2=1,n_2=1} + \omega_{l_3=2,n_3=1} = 635.9$ cm^{-1}, followed by the combination $\omega_{l_1=0,n_1=1} + \omega_{l_2=1,n_2=1} + \omega_{l_3=2,n_3=1} = 636.7$ cm^{-1}. The former has a strength 2.4 times larger (as illustrated in the figure by vertical lines) than the latter. The contributions of other modes are even smaller, being quenched by the size distribution function. The squares correspond to experimental data from Ref. 13. In this case the $L=1$ exciton energy has resonance radii $R = 3.93$, 4.08, 4.26, and 4.45 nm, which correspond to the incoming, two intermediate, and outgoing resonances, respectively.

C. Overall spectrum

An important test for any theoretical model involves the description of the overall measured spectrum at a given laser energy and for a specific mean radius of the nanocrystals. The measured relative strengths and spectral shapes of the overtones have to be described by the calculated Raman intensities. Figure 5(a) displays the evolution of the first-, second-, and third-order Raman processes of a single CdSe nanocrystal 1.9 nm in radius, as function of the laser energy and Raman shift. The incoming (I) and outgoing (O) resonances are indicated by arrows. The spectrum at $\hbar\omega_l = 2.575$ eV corresponds to incoming resonances for all investigated processes. It can be seen that the overtones of two phonons are stronger than the first-order peak, while the contribution of three phonons is absent in the scale of the figure.
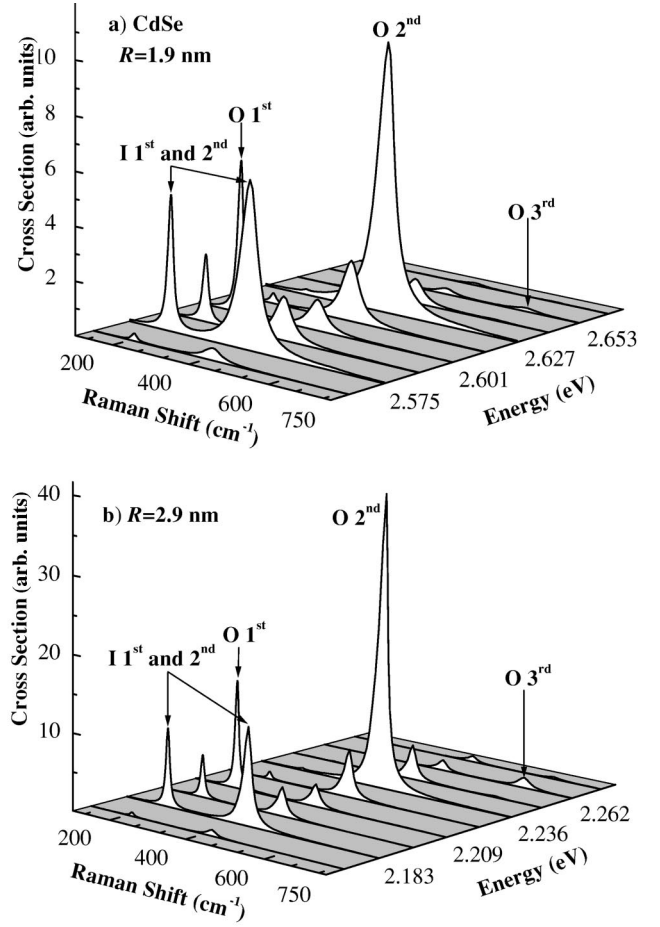

FIG. 5. Three-dimensional plot of the multiphonon resonant Raman cross section as a function of the Raman shift and laser energy. (a) Single spherical CdSe nanocrystal with 1.9 nm radius. (b) $R = 2.9$ nm. Incoming and outgoing resonances are labeled by I and O, respectively, and are indicated by arrows.

At $\hbar\omega_l = 2.600$ eV the spectra shows outgoing and intermediate resonances for the first and further order processes, respectively. Spectra at $\hbar\omega_l = 2.623$ eV and $\hbar\omega_l = 2.653$ eV present outgoing resonances for the two (414 cm^{-1} in the Raman shift) and the three phonons contributions, respectively. The two-phonon peak in the Raman cross section is stronger than the other ones, while the three-phonon outgoing resonance can be appreciated in this picture as a tiny peak in the Raman shift at 617 cm^{-1}, even weaker than the nonresonant second-order peak at 414 cm^{-1}. Figure 5(b) presents our calculation for a QD with $R = 2.9$ nm. As expected, the spectra are shifted to lower energy and incoming resonance is observed at $\hbar\omega_l = 2.183$ eV, while outgoing resonances are obtained at $\hbar\omega_l = 2.209$ eV, $\hbar\omega_l = 2.236$ eV, and $\hbar\omega_l = 2.262$ eV for the single phonon and the second and third overtones, respectively. It can be observed in Fig. 5 that for dots with larger radii, up to 2.9 nm, there is a slight increase in the third-order cross section corresponding to the outgoing resonance.

Figure 6 shows the measured MRRS of CdSe nanocrystals.[13] We have performed calculations of the MRRS within the framework of the model developed in this paper, in order to compare its ability to reproduce the experimental data. The parameters employed are the same as in the Figs. 2, 3, and 4. The total average Raman cross section is a
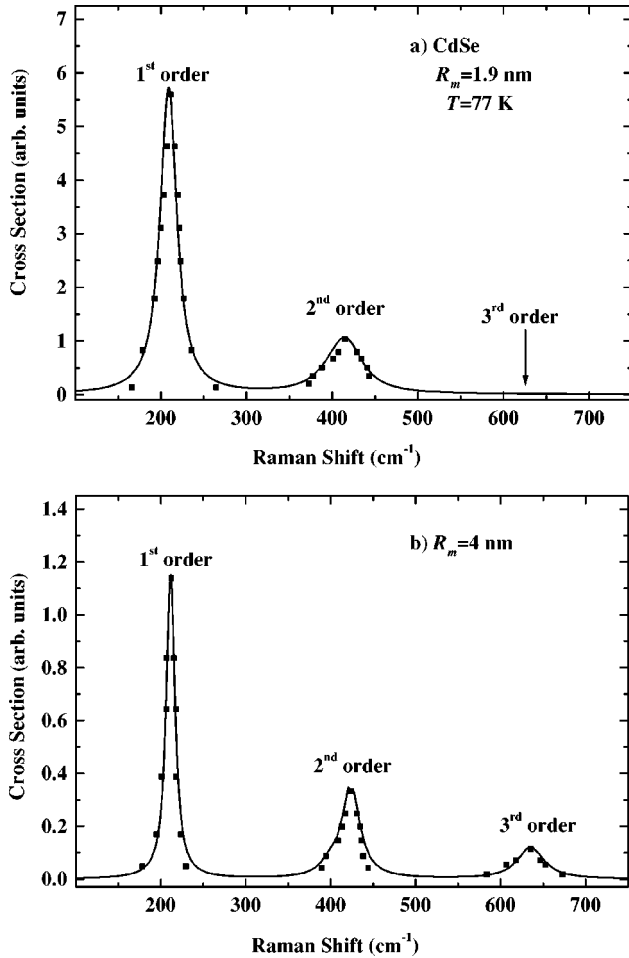
FIG. 6. Multiphonon Raman cross section of two ensembles of CdSe nanocrystals. A Gaussian radius distribution function with 10% FWHM is assumed for both ensembles. (a) Spectrum at $\hbar\omega_l = 2.572$ eV and $R_m = 1.9$ nm. (b) Spectrum at $\hbar\omega_l = 2.184$ eV and $R_m = 4.0$ nm. Experimental data are represented by black squares and theoretical calculations by the solid lines. In the calculation the parameters employed are the same as in Figs. 2–4. The relative overtone intensities have been fitted by weighting the ith order cross sections $S_D^{(i)}$ [see Eq. (13)] according to the equation $S_D = A S_D^{(1)} + S_D^{(2)} + B S_D^{(3)}$. In (a) A=13 and B=1, while in (b) A=2.55 and B=1/4.75.

sum of the first-, second-, and third-order cross sections $S_D^{(i)}$ (i=1,2, and 3) using Eq. (13). In Fig. 6(a) and 6(b) the calculations and the experimental spectra have been normalized at $\omega_s = 414$ cm^{-1}, corresponding to the second-order process. To fit the experimental data, the calculated first-order cross section was multiplied by a factor of 13 and 2.55 for QD's with $R_m = 1.9$ nm [Fig. 6(a)] and 4.0 nm [Fig. 6(b)], respectively. The evaluated third-order cross section has been divided in Fig. 6(b) by a factor of 4.74. The theoretical predictions are shown in Fig. 6 as solid lines and the experimental data as black squares. Semiquantitative agreement between theory and measured scattering intensities is found without invoking nonintrinsic physical interactions to obtain the relative intensities of the Raman overtone. Nevertheless, to provide a completely quantitative description of the overall measured spectra, a correction prefactor ranging from three to ten has been inserted in Eq. (3). Despite these ''fudge'' factors, the agreement between the measured spec-

tra and those calculated by us is significantly better than with the mechanisms used hitherto in order to describe MRRS in QD's, as will be discussed in the next section. The spectrum of Fig. 6(a) (an ensemble of dots with $R_m = 1.9$ nm) does not present the overtones with three phonons. In this case the calculation shows that the third-order Raman cross section is 10^3 times smaller than the second-order contribution, in agreement with the experimental observation.

The differences of the relative overtone intensities between the theory and the experimental data can be explained as follows. First, an interesting feature is observed in the calculated Raman cross section where the intensity of the first-order process is, in general, smaller than that corresponding to two overtones. This result can be due to our simplified electronic band model, where the valence bands have been assumed to be parabolic, without band mixing. The one-LO-phonon Raman cross section is known to be very sensitive to the difference between the electron and hole wave functions.[22,32] The decompensation between electron and hole densities can be affected by either the electron-hole Coulomb interaction, different confinement barriers for the electron and hole, or band-mixing effects. Using different confinement radii for the electron and hole, up to 10% difference to simulate the penetration of the wave function into the matrix and in the framework of the infinite barrier with parabolic band model, we have found huge values for the first-order Raman intensities. The one-phonon absolute intensity is an interesting and delicate problem that merits an independent study and also experimental measurements of absolute values. On the other hand, higher-order processes are possible through different channels, with participation of phonons with $l_p \geq 1$ and excitons of different symmetries. In this case the Raman absolute values are not sensitive to the electron-hole decompensation effect. Notice that the relation between the first- and second-order intensities is not determined simply by a Huang-Rhys parameter[33,34] due to dominant additional scattering channels allowed in the second-order process. Second, the experimental data are taken from a commercial filter, which was assumed to contain CdSe nanocrystalites with a Gaussian distribution for R and a relative size dispersion of 10%. The mean radius was estimated from the maximum of the absorption coefficient and the formula $E(R_m) = \hbar^2\pi^2/2\bar{\mu}R_m^2$ for the free electron-hole pair completely confined model energy.[13] The R_m value depends rather critically on the exact electron-hole energy function, which is itself sample dependent.[10] This procedure is not very accurate when used to deduce the QD radius by comparing the energies to experimental data. We have studied the influence of the size distribution function on the MRRS for a fixed laser photon energy. There is a set of radii for which the nanocrystals are in either incoming, intermediate, or outgoing resonance with different exciton levels. The cross section is the average of the cross sections for those radii, weighted by the size distribution function. We found that for $R_m = 2.9$ nm, the second-order cross section is 70 times larger than the third-order one, but 5 times smaller for $R_m = 4.0$ nm. It is possible to obtain the ratio of two- to three-phonon intensities using as a fit parameter the mean radius. Instead, we chose to multiply the overtone intensity by a fitting factor (of the order of 10) when comparing with available MRRS experiments.

D. Huang-Rhys factor

The success in reproducing the MRRS experiments and the relative overtone intensities indicates clearly that any theoretical model used to describe the Raman spectra needs to include all excitonic and phonon channels that contribute to light dispersion in quantum dots. Notice, that large values of the Huang-Rhys (HR) factor are not invoked in the present formalism to reproduce the experimental data. The Huang-Rhys factor taking into account excitonic states is evaluated with the equation[17]

$$\Delta^2 = \sum_p \left| \frac{\langle N,L,M,P | e[\varphi_F^p(\mathbf{r}_e) - \varphi_F^p(\mathbf{r}_h)] | P,M,L,N \rangle}{\hbar \omega_p} \right|^2 .$$

A direct calculation of Δ^2 for a CdSe QD ($L=0, M=0, P=1$, and $l_p = 0$ phonon) gives values about 10^{-3}.

Several authors have studied the electron-phonon coupling strength in nanocrystals, e.g., CdSe,[11–15,35] CuCl,[36] CuBr,[37] and CdS.[38] Usually, Raman and luminescence spectra have been interpreted within the Franck-Condon model. The idea behind this approach is that for any instantaneous ion position, the electronic subsystem is in a stationary state. Hence, the electron-lattice interaction leads to instantaneous modifications of the electronic stationary states without occurrence of any electronic transitions. Moreover, the exciton-phonon coupling factor is identified with the Huang-Rhys factor, using this as a fitting parameter for the relative intensities of different orders in Raman spectra. The calculations of the Huang-Rhys parameter for intrinsic exciton states in CdSe[14] and PbS[17] nanocrystals have given values that are too small compared with those needed to explain the experimental results. In order to understand this disagreement, other extrinsic mechanisms have been invoked such as: donorlike exciton with the hole localized at the dot center,[18] hole traps at the surface with a trapping radius obtained from a fitting procedure,[15] or placing an extra charge in the nanocrystal center.[14] However, no definite evidence has been given of the dominating role of extrinsic states in Raman processes in quantum dots, while both types of intrinsic and extrinsic states have certainly been observed in luminescence experiments.[8,15,39,40] Also, a nonadiabatic theory[41] has been invoked to obtain better agreement with the experimental data. The calculations presented here explain the observed large overtone intensities in Raman spectra without resorting to any mechanism other than intrinsic and adiabatic ones.

The explanation of why such large values of Huang-Rhys parameter have been obtained from experimental data is found in the simplified theory used to interpret the experiments. The Franck-Condon scheme is particularly useful for small molecules, where forces acting on ions depend strongly on the electronic state. The Raman polarizability can be split in two contributions: Albrecht's $\tilde{A}$ and $\tilde{B}$ terms.[22,42] The largest contribution comes from Albrecht's $\tilde{A}$ term, accounting for multiphonon processes. The term $\tilde{A}$ in conjunction with the offset oscillators model (this model states that the ionic potential energy parabola is displaced by an amount Δ in units of the oscillator length) is used to fit the experimental data.[13,17,35,36] The offset square Δ^2, taken as a fitting parameter, is then interpreted as the Huang-Rhys parameter. However, if the resonant Raman scattering is mediated by extended states, as usually occurs in large molecules

and solids, the vibrational states do not depend on a single electronic excitation (which means that $\Delta^2 \simeq 0$). In this case the $\tilde{A}$ term contributes only to elastic scattering. Accordingly, the $\tilde{B}$ term, calculated as a perturbation correction to $\tilde{A}$, is exactly the result of Ref. 27, i.e., the first-order Raman process. The overtones can be properly described if higher corrections to the $\tilde{A}$ term are taken into account. We must remark that Albrecht's $\tilde{A}$ term cannot explain the optical vibrational Raman scattering if the intermediate electronic excitations are extended states. Any estimation of the Huang-Rhys parameter based on this model should give, in principle, artificially large values. A definite test for the inadequacy of the HR factor treatment could be obtained by measuring absolute values of Raman efficiencies. A theory that satisfactorily fits the experimental absolute values of the resonance profile could clarify the role of the Huang-Rhys parameter and the exciton-phonon interactions in QD's.

IV. CONCLUSIONS

We have presented a general treatment for calculating the multiorder resonant Raman-scattering spectra of spherical semiconductor nanocrystals. The treatment considers confined Wannier-Mott excitons in the effective-mass approximation and the full symmetry of the optical vibrations through the coupling between the electrostatic potential and mechanical displacement parts of the problem. The theory is particularly important for very small QD's where a Fröhlich exciton-phonon interaction operator takes into account the mixing between confined and interface modes through mechanical and electrostatic boundary conditions. In our calculation, the effects of identical phonons contributing to the Raman cross section for a given order have been considered. An important feature of the Raman profile is the presence of outgoing resonance peaks larger than the incoming ones for all scattering processes. Figure 5 shows that the strongest Raman line corresponds to the outgoing resonance for the second-order process. The physical reasons are the following: (1) First-order scattering is quasiforbidden; (2) The Fröhlich coupling constant is smaller than one for Group-II–VI semiconductors, which favors the second order in comparison with the third-order processes; (3) For the QD radii studied here, the intermediate states, in general, are not in resonance simultaneously with the outgoing channels.

The numerical results for CdSe nanocrystals presented here do not only reproduce the main trends of the experimental results, but also teach us that in order to extract comprehensive information from the comparison between theory and MRRS experiment in nanocrystals, it is necessary to (a) precisely tune the resonance conditions, (b) to know the exciton energy levels, and (c) to know the size distribution function of the nanocrystals. We have shown that the numerical results for the Raman cross section are very sensitive to all these parameters. The above facts have been already pointed out by Scamarcio *et al.*,[35] where the authors tuned simultaneously the laser frequency and the dot radii while keeping the resonance conditions.

The problem of the traditional interpretation of MRRS spectra in terms of the Huang-Rhys parameter[34] has been stressed, concluding that multiphonon Raman scattering can be correctly described if a detailed analysis of the resonance

conditions, vibrational modes, and excitonic states in the ensemble is carried out. It is shown that a treatment based on a Huang-Rhys parameter is not appropriate for describing the relative overtone intensities since other significant scattering and interference channels have to be taken into account in the Raman cross section.

In order to fit the intensity of the one-phonon process, a better knowledge of the exciton wave function is needed. Due to the charge decompensation effect, the absolute one-phonon scattering intensity depends strongly on the details of the exciton wave function.[32] To test our model, calculations and comparison to experiments for other materials are currently in progress.

*Permanent address: Departamento de Física, Universidad de Oriente, Patricio Lumumba, Santiago de Cuba, Cuba.

†Present address: Instituto de Materiales y Reactivos, Universidad de La Habana, Vedado 10400, La Habana, Cuba.

‡Permanent address: Departamento de Física Teórica, Universidad de La Habana, Vedado 10400, La Habana, Cuba.

[1] U. Woggon and S. V. Gaponenko, Phys. Status Solidi B **189**, 285 (1990).

[2] M. Bruchez, Jr., M. Moronne, P. Gin, S. Weiss, and A. P. Alivisatos, Science **281**, 2013 (1998); W. C. W. Chan and S. Nie, Science **281**, 2016 (1998).

[3] A. Ekimov, J. Lumin. **70**, 1 (1996).

[4] C. B. Murray, C. R. Kagan, and M. G. Bawendi, Science **270**, 1335 (1995).

[5] A. A. Guzelian, U. Banin, A. V. Kadanovich, X. Peng, and A. P. Alivisatos, Appl. Phys. Lett. **69**, 1432 (1996).

[6] D. Bertram, Phys. Rev. B **57**, 4265 (1998).

[7] Yu. A. Pusep, G. Zanelatto, S. W. da Silva, J. C. Galzerani, P. P. Gonzalez-Borrero, A. I. Toropov, and P. Basmaji, Phys. Rev. B **58**, R1770 (1998).

[8] S. A. Empedocles, D. J. Norris, and M. G. Bawendi, Phys. Rev. Lett. **77**, 3877 (1996).

[9] D. J. Norris, A. Sacra, C. B. Murray, and M. G. Bawendi, Phys. Rev. Lett. **72**, 2612 (1994).

[10] C. Trallero-Giner, A. Debernardi, M. Cardona, E. Menéndez-Proupin, and A. I. Ekimov, Phys. Rev. B **57**, 4664 (1998).

[11] S. Schmitt-Rink, D. A. B. Miller, and D. S. Chemla, Phys. Rev. B **35**, 8113 (1987).

[12] A. P. Alivisatos, T. D. Harris, P. J. Carrol, M. L. Steigerwald, and L. E. Brus, J. Chem. Phys. **90**, 3463 (1989).

[13] M. C. Klein, F. Hache, D. Ricard, and C. Flytzanis, Phys. Rev. B **42**, 11 123 (1990).

[14] S. Nomura and T. Kobayashi, Phys. Rev. B **45**, 1305 (1992).

[15] M. G. Bawendi, P. J. Carroll, W. L. Wilson, and L. E. Brus, J. Chem. Phys. **96**, 946 (1992).

[16] In quantum dots the quantized optical lattice vibrations are normally called phonons or vibrons. Strictly, phonons are **k**-dependent quasiparticles, while vibrons are quantum nonadiabatic oscillations in molecules. For the sake of simplicity, in this paper we use the word ''phonons.''

[17] T. D. Krauss and F. K. Wise, Phys. Rev. B **55**, 9860 (1997).

[18] J. C. Marini, B. Stebe, and E. Kartheuser, Phys. Rev. B **50**, 14 302 (1994).

[19] J. J. Shiang, S. H. Risbud, and P. Alivisatos, J. Chem. Phys. **98**, 8432 (1993).

[20] V. I. Belitsky, A. Cantarero, S. T. Pavlov, M. Cardona, I. G. Lang, and A. V. Prokhorov, Phys. Rev. B **52**, 11 920 (1995), and references therein.

[21] D. J. Mowbray, M. Cardona, and K. Ploog, Phys. Rev. B **43**, 11 915 (1991); L. I. Korovin, S. T. Pavlov, and B. E. Eshpulator, Phys. Solid State **35**, 788 (1993), and references therein.

[22] M. Cardona, in *Light Scattering in Solids II*, edited by M. Cardona and G. Güntherodt, *Topics in Applied Physics*, Vol. 50 (Springer-Verlag, Heidelberg, 1982).

[23] W. Hayes and R. Loudon, *Scattering of Light by Crystals* (Wiley, New York, 1978).

[24] E. Menéndez, C. Trallero-Giner, and M. Cardona, Phys. Status Solidi B **199**, 81 (1997).

[25] E. Menéndez-Proupin, C. Trallero-Giner, and A. García Cristobal, Phys. Rev. B **60**, 5513 (1999).

[26] E. Roca, C. Trallero-Giner, and M. Cardona, Phys. Rev. B **49**, 13 704 (1994).

[27] M. P. Chamberlain, C. Trallero-Giner, and M. Cardona, Phys. Rev. B **51**, 1680 (1995).

[28] D. M. Brink and G. R. Satcher, *Angular Momentum* (Clarendon Press, Oxford, 1968).

[29] Values of Γ_1^{ex} have not been reported, but they should be larger than Γ_0^{ex} to account for relaxation to the lower excitonic states. For the linewidth of excited states we assumed the criterium followed in several bulk semiconductors to fit absolute Raman values [A. García Cristobal, A. Cantarero, C. Trallero-Giner, and M. Cardona, Phys. Rev. B **58**, 10 443 (1998) and references there in] where Γ_n^{ex} ranges from 1 to 3 times Γ_0^{ex}. The values of 15 and 8 meV are far from well established. A realistic determination of Γ_0^{ex} and Γ_1^{ex} could be performed by measuring of the resonance profile of a monodisperse QD's ensemble.

[30] Landolt-Börnstein, *Numerical Data and Functional Relationships in Science and Technology*, edited by O. Madelung (Springer-Verlag, Berlin, 1986), Vol. III/22.

[31] C. Trallero-Giner, F. García Moliner, V. R. Velasco, and M. Cardona, Phys. Rev. B **45**, 11 944 (1992).

[32] E. Menéndez-Proupin, J. L. Peña, and C. Trallero-Giner, Semicond. Sci. Technol. **13**, 871 (1998).

[33] K. Huang and A. Rhys, Proc. R. Soc. London, Ser. A **204**, 406 (1950).

[34] R. Merlin, G. Güntherodt, R. Humphreys, M. Cardona, R. Suryanarayanan, and F. Holtzberg, Phys. Rev. B **17**, 4951 (1978).

[35] G. Scamarcio, V. Spagnolo, G. Ventruti, M. Lugara, and G. C. Righini, Phys. Rev. **53**, R10 489 (1996).

[36] A. V. Baranov, S. Yamaguchi, and Y. Matsumoto, Phys. Rev. B **56**, 10 332 (1997); T. Itoh, M. Nishijima, A. I. Ekimov, C. Gourdon, Al. L. Efros, and M. Rosen, Phys. Rev. Lett. **74**, 1645 (1995).

[37] K. Inoue, K. Toba, A. Yamanaka, A. V. Baranov, A. A. Onushchenko, and A. V. Fedorov, Phys. Rev. B **54**, R8321 (1996).

[38] W. Jungnickel, F. Henneberger, and J. Plus, in *Proceedings of the 22nd International Conference of Semiconductors, Vancouver, B.C., 1994*, edited by D. J. Lockwood (World Scientific, Singapore, 1995), Vol. III, p. 2011.

[39] Al. L. Efros, M. Rosen, M. Kuno, M. Nirmal, D. J. Norris, and M. Bawendi, Phys. Rev. B **54**, 4843 (1996).

[40] Al. L. Efros and A. V. Rodina, Phys. Rev. B **47**, 10 005 (1993).

[41] V. M. Fomin, V. N. Gladilin, J. T. Devreese, E. P. Pokatilov, S. N. Balaban, and S. N. Klimin, Phys. Rev. B **57**, 2415 (1998).

[42] A. C. Albrecht, J. Chem. Phys. **34**, 1476 (1961).